ELSEVIER

Cement & Concrete Composites 24 (2002) 415–426

Cement & Concrete Composites

www.elsevier.com/locate/cemconcomp

Depth-related variation in conductivity to study cover-zone concrete during wetting and drying

T.M. Chrisp [a,*], W.J. McCarter [a], G. Starrs [a], P.A.M. Basheer [b], J. Blewett [a]

[a] Department of Civil and Offshore Engineering, Heriot Watt University, Edinburgh EH14 4AS, Scotland, UK
[b] School of Civil Engineering, The Queen's University of Belfast, Belfast BT7 1NN, Northern Ireland, UK

Abstract

In situ electrical property measurements are used to study cover-zone concrete under a cyclic wetting and drying regime. OPC concrete and OPC with partial replacement with GGBS and PFA were used in the experimental programme with samples exposed to water and chloride solution. Monitoring the variation of electrical properties at discrete points within the surface 50 mm, during absorption and drying, provides information on water and ionic penetration into the cover zone, drying response, and evidence of continuing hydration and pozzolanic reaction.

Keywords: Cover zone; Durability; Monitoring; Conductivity; Absorption

1. Introduction

It is paradoxical that while water is essential for cement hydration, it plays a major role in virtually all reinforced concrete deterioration process. For example, chloride ingress; freeze–thaw damage; sulphate attack, alkali-aggregate reaction all depend on the presence of water. It is not surprising, therefore, that the study of water movement, particularly within cover-zone concrete (i.e. the covercrete) is an area of considerable importance. There clearly exists a need to determine quantitatively those near-surface characteristics of concrete that promote the ingress of gases or liquids containing dissolved contaminants. To this end, surface-applied techniques (e.g. initial surface absorption test – ISAT) have been developed to determine the water and gas permeation properties of cover-zone concrete (see, for example, [1–10]). The results from such tests are then used to assess durability.

Deterioration processes comprise an initiation period and a propagation period. The initiation period is characterised by changes that occur within the concrete in response to the exposure environment. Initiation continues until a stage is reached when damage begins to propagate. The propagation period begins at a point in time defined when a particular event occurs (e.g. loss of steel passivity) and continues until a specified limit state is reached [11,12]. The initiation and propagation stages of a deterioration process result from a complex interaction of physical, chemical and electrochemical phenomena. Prediction of the field performance of reinforced concrete thus requires numerous data inputs, in particular, the response of the covercrete to the changing micro-environment in the vicinity of a specific structural element or part of a structure. Cover-zone transport mechanisms, their variation through the covercrete, drying characteristics and the temporal change in these properties, all influence reinforced concrete durability.

In situ monitoring of cover-zone concrete – *in real time* – could assist in making realistic predictions as to the in-service performance of the structure, likely deterioration rates for a particular exposure condition, compliance with the specified design life and as an early warning indicator of incipient problems. Set against this background the work below details development in the application of electrical measurements to study water and ionic movement within cover-zone concrete. The current study, which forms part of a long-term study on chloride induced corrosion, presents data for specimens undergoing a cyclic wetting regime with water and water containing dissolved chlorides.

* Corresponding author. Tel.: +44-131-451-3595; fax: +44-131-451-5078.
E-mail address: chrisp@civ.hw.ac.uk (T.M. Chrisp).

0958-9465/02/$ - see front matter
PII: S0958-9465(01)00073-7

2. Experimental

2.1. Materials, samples and curing

Mixes were chosen to meet the requirements for extreme exposure conditions according to British Standard BS8110: 1985: Part 1 and also complied with mixes used in a field-exposure programme which forms part of the long-term study noted above. Table 1 presents the concrete mix details, together with the mean 7- and 28-day compressive strength (F_7 and F_{28}) determined on 100 mm cubes. Dredged river gravel and matching fines (Zone M to British Standard BS812: Part 103) were used throughout. The binders comprised ordinary Portland cement (OPC to BS12), ground granulated blast-furnace slag (GGBS to BS6699) and pulverised fuel ash (PFA to BS3892: Part 1).

Specimens were $300 \times 300 \times 125$ mm (thick) blocks, with the working face cast against plywood formwork which had been given a coat of proprietary release agent prior to casting (Nufins Formstrike). An electrode array, described below, was placed in the surface 50 mm (see Fig. 1(a)). On demoulding, the samples were wrapped with damp hessian and polythene for a period of seven days. All surfaces, apart from the surface cast against the formwork that was to be used as the exposed working surface, were then sealed with several coats of an epoxy-based paint to ensure one-dimensional drying. They were left in a laboratory (22 ± 2 °C; 50–55% RH) for a period of five weeks before being subjected to cyclic wetting and drying. Six specimens were cast for each mix.

In addition to these specimens, a further nine samples (three per mix) were fabricated and after demoulding were continuously moist cured throughout the test period. This set of samples had an embedded electrode array and served to benchmark changes in electrical response purely due to hydration effects.

2.2. Electrical measurements

Electrical conductance (reciprocal of resistance) measurements were obtained at discrete points within the cover zone of concrete samples by embedding a miniature electrode array in the surface 50 mm of the reinforced concrete slabs. This is a refinement on other embedded electrode systems [13–15] and further details can be obtained in [16]. In summary, the probe comprised seven electrode pairs mounted on a small Plexiglas former; each electrode consisted of a stainless steel pin (1.2 mm in diameter) which was sleeved to expose a

Table 1
Summary of concrete mixes

Mix Ref.	OPC (kg/m^3)	PFA (kg/m^3)	GGBS (kg/m^3)	20 mm (kg/m^3)	10 mm (kg/m^3)	Fines (kg/m^3)	WRA (l/m^3)	w/b	F_7 (MPa)	F_{28} (MPa)
OPC	460	–	–	700	350	700	1.84	0.4	57	70
GGBS	270	–	180	700	375	745	3.60	0.44	31	53
PFA	370	160	–	695	345	635	2.65	0.39	33	58

(WRA = water reducing agent; w/b = water–binder ratio).

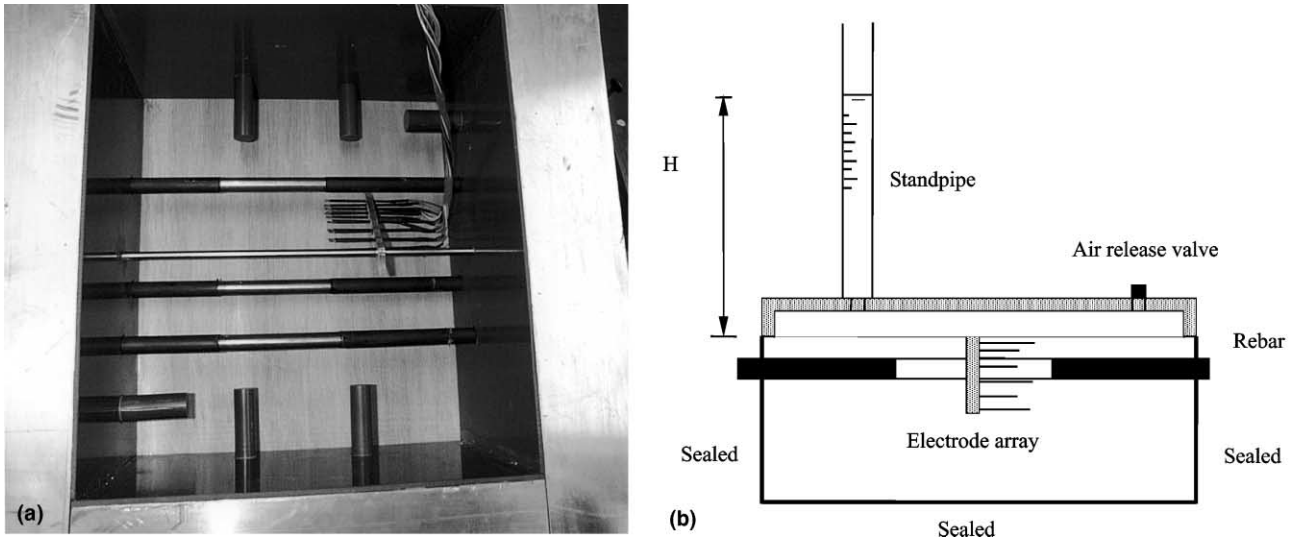

Fig. 1. (a) Electrode array, steel bars, stainless steel (s/s) counted electrode and humidity cavities prior to casting; and (b) schematic diagram of testing arrangement (rebars at 30 and 45 mm; s/s counter electrode, and humidity cavities omitted for clarity).

5 mm tip; in each electrode pair the pins had a (horizontal) centre to centre spacing of 5 mm. The pairs of electrodes were positioned at 5, 10, 15, 20, 30, 40, 50 mm from the exposed surface, thereby enabling electrical measurements to be taken at discrete points within the cover zone and parallel to the test surface (Fig. 1(a)). A thermistor was also mounted on the former to allow measurement of the covercrete temperature (although in the work presented, tests were carried out within the confines of a temperature-controlled laboratory). The electrode arrays were also calibrated in solutions of known conductivity enabling the measured conductance to be converted to *conductivity* [16]. The former was secured within each of the samples.

Changes in resistance between pairs of electrodes were measured using an auto-ranging impedance analyser (Hewlett Packard 4263B LCR meter) interfaced to a multiplexing unit (Hewlett Packard 34970A). The system was controlled by a PC using HPVEE software. Preliminary studies optimised the excitation signal at a frequency of 1 kHz and signal amplitude of 1 V and ensured electrode polarisation effects were reduced to negligible proportions [17] for all mixes.

The samples also had three 12.5 mm diameter steel bars positioned to have 15, 30 and 45 mm cover, with bars sleeved to expose a 100 mm central portion (see Fig. 1(a)). A stainless steel bar was also placed within the samples to facilitate linear polarisation measurements at a later stage. Half-cell measurements were made on each bar over the test period. (Note: humidity cavities were also cast into the specimens, however, results are not discussed in this current work.)

2.3. Cyclic testing regime

Each sample set for cyclic testing was divided equally with one sub-set of specimens exposed to wetting cycles with water and the other subjected to wetting cycles of 1 M NaCl (1.0 M: 58.4 g/l). The cyclic regime started six weeks after demoulding with wetting and drying cycles comprising approximately 48-h absorption followed by a period of drying (generally about seven weeks, although this was accidentally reduced at approximately 450 days). Fig. 1(b) displays a schematic of the testing arrangement with an average head, H, of 400 mm maintained on the sample over the absorption period.

3. Results and discussion

Conductivity measurements were recorded across electrode pairs within the cover zone over multiple cycles of wetting and drying. However, due to the amount of data collected, only a selection of results are presented to highlight the information that can be obtained from electrical monitoring. Data are also presented for those specimens undergoing continuous moist curing with all electrical measurements presented at 20 °C. Volumetric absorption measurements were recorded during the period of wetting.

3.1. Electrical conductivity during wetting and drying

The periods of wetting and drying are clearly evident from Figs. 2(a)–(c) (water) and Figs. 3(a)–(c) (NaCl solution); for clarity, only the response from depths of 5, 10, 15, 30, 50 mm is displayed on these figures. As water is drawn into the partially saturated cover zone by capillarity, the wetting portion of the cycle is clearly evident for all mixes and is characterised by an increase in conductivity, although the prominence of this increase diminishes with increasing depth and time. Where conductivity increases signify that the wetting front has penetrated into the zone of influence of the electrical field between that particular electrode pair. This can be explained with reference to the schematic diagram presented in Fig. 4. In position I indicated, the wetting front is distant from the region of influence of the electrical field between the electrode pair and hence little change in conductivity would be detected. In position II, the wetting front has now advanced into the zone of influence of the electrical field and, eventually, moves just beyond its influence as depicted in position III in Fig. 4. Over this period, the conductivity of the concrete will increase as the wetting front eventually makes contact with the electrodes. Finally, in position IV, the wetting front has now advanced beyond the zone of influence of the electrical field and the conductivity would now attain a relatively constant value with time. Comparing Figs. 2 and 3, the influence of NaCl in the invading water is also detected by the conductivity response of the covercrete. Conductivity values over the surface 0–10 mm are enhanced in comparison to their water-exposed counterparts. These aspects are discussed below in more detail.

In studying the depth-related response, it is informative to present the variation in conductivity through the cover zone at salient points in time. For example, Figs. 5(a)–(c) present conductivity profiles prior to, and immediately after, both the 'initial' wetting cycle and the 'final' wetting cycle i.e. at the beginning and end of the time period presented in Fig. 2. This is only presented for water-exposed specimens. Since drying involves transfer of water vapour from within the covercrete to the exposed surface, a moisture gradient will be established through the cover zone. The conductivity profiles just prior to the absorption cycle increase with distance from the exposed surface and reflect the increasing degree of pore saturation from the exposed surface.

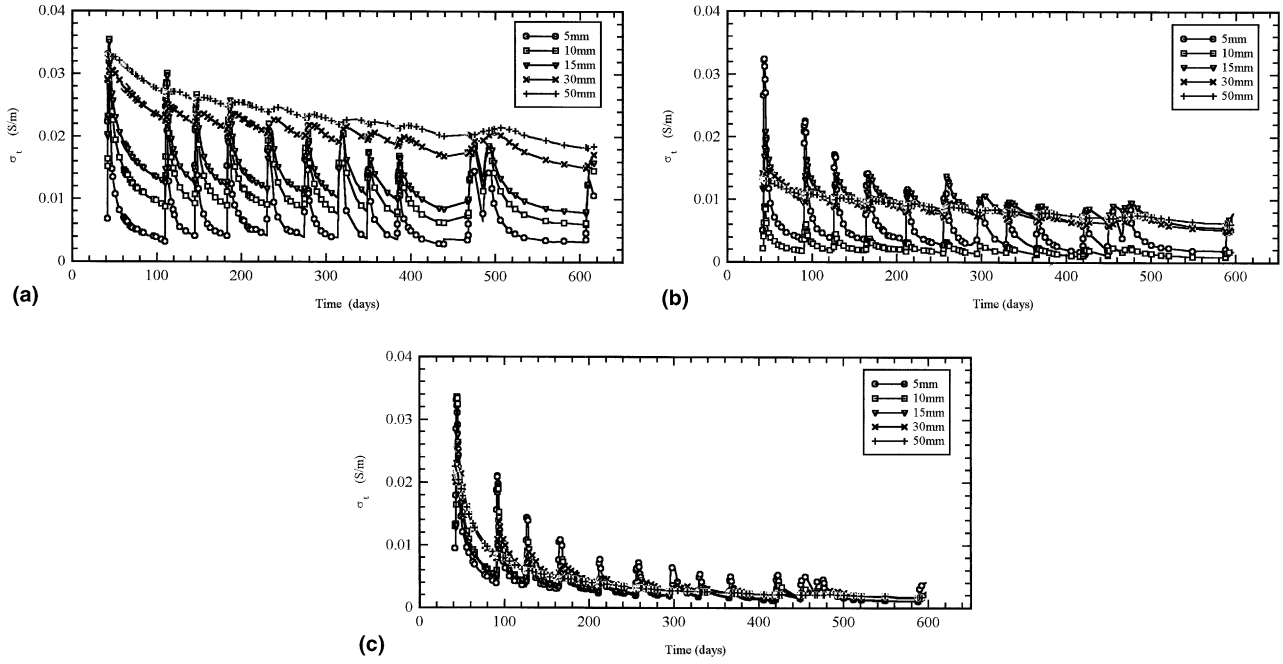

Fig. 2. Conductivity (σ_t) versus time for specimens undergoing cyclic wetting and drying (water) for (a) OPC, (b) GGBS, and (c) PFA.

Conductivity values measured at a depth of 5 mm can be up to five times lower than those measured at 50 mm.

After subsequent wetting, the penetration of the wetting front into the cover zone increases conductivity values relative to the respective values prior to wetting. For example, at 5 mm, the conductivity can increase by up to an order of magnitude after absorption. The influence of drying and wetting effects diminish with depth and the electrode pair at 50 mm display little marked response to wetting and drying regime applied at the surface, only showing a decrease in conductivity with time over the test period presented. The latter is attributed to on-going hydration and pozzolanic reaction, indicating the continual refinement in pore structure

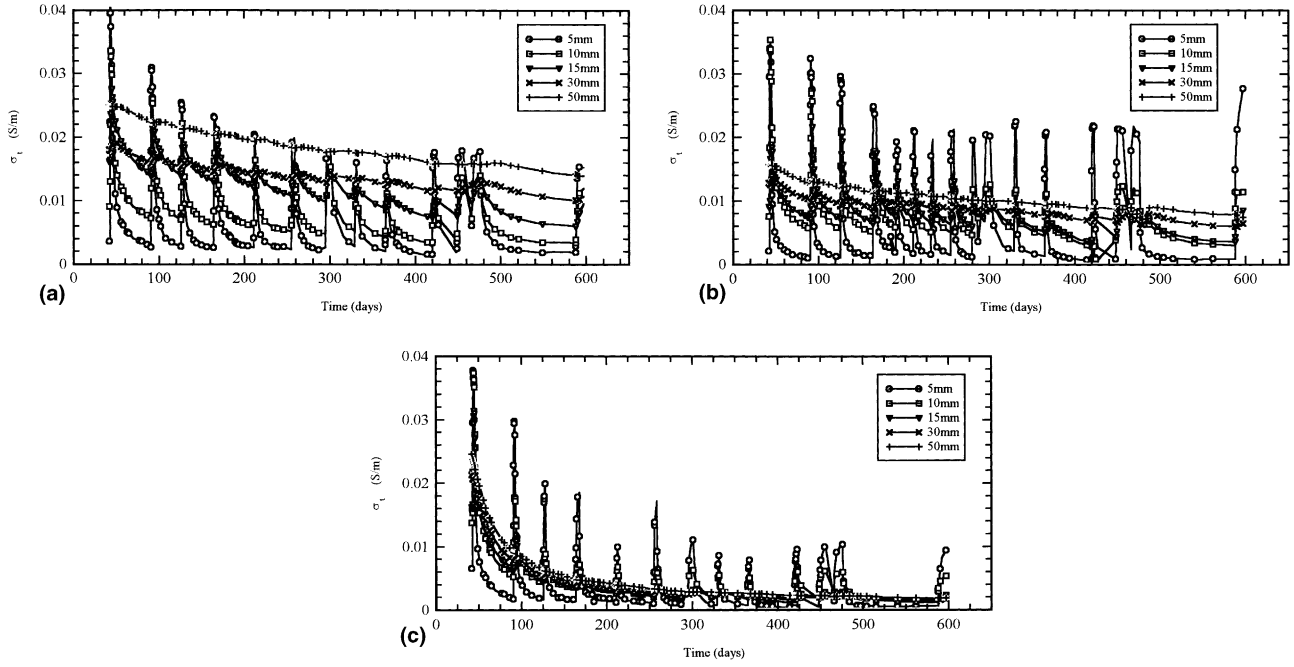

Fig. 3. Conductivity (σ_t) versus time for specimens undergoing cyclic wetting and drying (NaCl) for (a) OPC, (b) GGBS, and (c) PFA.

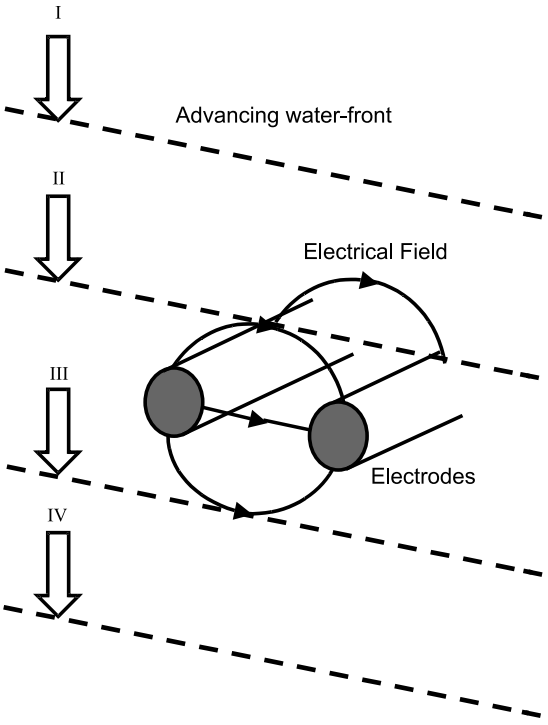

Fig. 4. Schematic showing the wetting front moving into the cover-crete.

within the cover zone during in post-curing period. This effect is particularly evident in the GGBS and PFA mixes. Regarding the PFA mix, the conductivity at 50 mm decreases by more than an order of magnitude between the first and last cycles.

That point where the conductivity profiles before and after wetting become coincident is taken as an estimate of the depth of the surface zone most influenced by drying and wetting action (see Fig. 6). This region has been termed the *convective zone* and normally based on internal RH measurements [18]. From the conductivity profiles in Fig. 5, the convective zone is in the region of ≈25–30 mm for all mixes after the initial absorption cycle. At the end of the final absorption cycle, the convective zone is reduced, particularly in the case of the PFA mix and due to microstructural changes resulting from hydration etc. as noted above. The movement of water into the convective zone will be by capillarity. Such a process is relatively rapid and the practical significance in identifying the convective zone after a period of drying is that it represents that portion of the cover which is not contributing to the protection of the steel – this could be considered 'lost' cover.

The conductivity profiles also allow estimation of the conductivity of the concrete at reinforcement level. Once passivity has been lost, the electrical properties of the concrete in the vicinity of corrosion activity play an important role in corrosion dynamics [19–22], and conductivity/resistivity thresholds have been published in this respect [23].

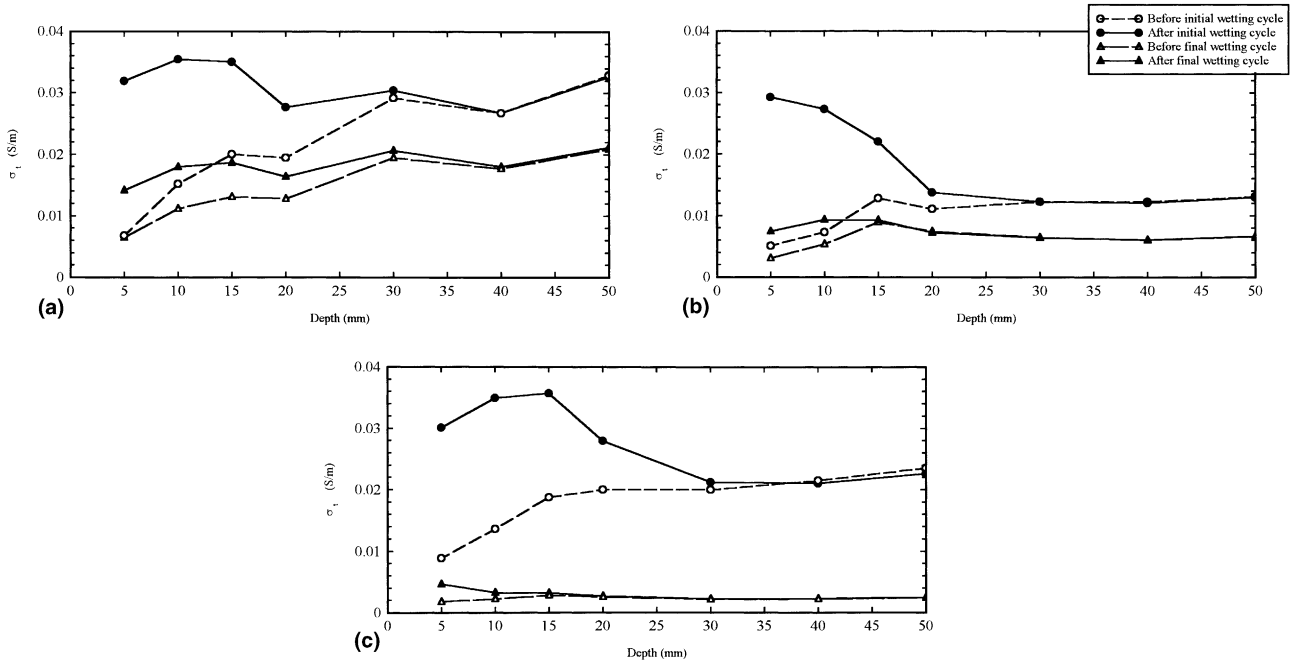

Fig. 5. Conductivity profiles through surface 50 mm before and after wetting for water-exposed specimens for (a) OPC, (b) GGBS, and (c) PFA (initial and final cycles).

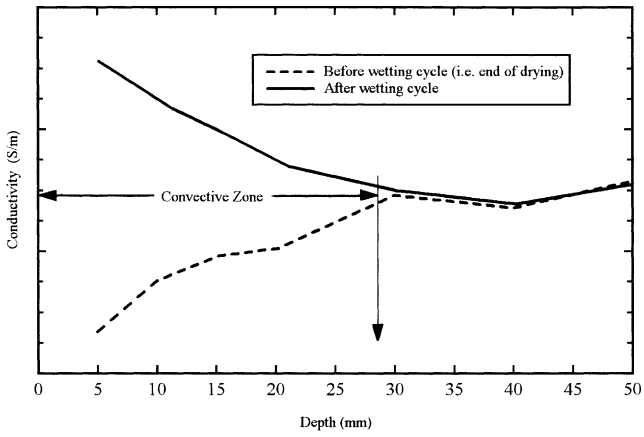

Fig. 6. Schematic diagram showing convective zone determined from conductivity profiles.

3.2. Electrical measurements during continuous moist curing

Fig. 7 presents the electrical response resulting for specimens undergoing continuous moist curing from time of demoulding. The curves are self-explanatory as the conductivity decreases with time, particularly the PFA mix. It is of interest to note that the responses after the initial 42 days follow those obtained at the 50 mm level within the respective specimens undergoing a cyclic regime. This would corroborate the assertion above that the response at this depth, at this stage, reflects hydration effects.

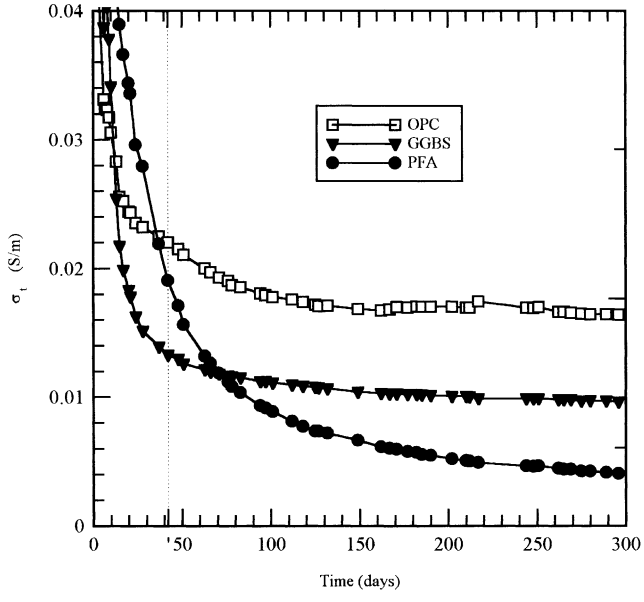

Fig. 7. Conductivity (σ_t) versus time for continuous moist curing.

3.3. Cumulative volumetric gain

The cumulative absorption data, expressed as volumetric gain per unit area of inflow surface (i mm^3/mm^2), are presented in Figs. 8 and 9 for, respectively, water and NaCl solution. For illustrative purposes only, data are presented for the initial six absorption cycles. Over the wetting period, the data display deviation from the classic $\sqrt{time}$ relationship and can be represented by a quadratic equation of the form $i = at + b\sqrt{t} + c$, where a, b and c are determined empirically [24]. There is a decrease in i with time, particularly between the 1st and 2nd wetting cycles, and attributable to continuing hydration and detected from conductivity measurements. Interestingly, the NaCl-exposed specimens show a lower volumetric gain than their water-exposed counterparts. This could be explained by a combination of several effects – further pore structure refinement due to chloride binding effects [25,26]; crystallisation of NaCl in the pores, and increased viscosity of the salt solution.

3.4. Normalised conductivity

Electrical conductivity measurements are presented in a dimensionless format by *normalising* all conductivity values by the value obtained at a depth of 50 mm, i.e.

$$N_C = \frac{\sigma_t}{\sigma_{t,50}}, \tag{1}$$

where N_C is the normalised conductivity; σ_t is the conductivity across a particular electrode pair at time, t, after the start of the initial absorption test, and $\sigma_{t,50}$ is the value of conductivity across the electrode pair positioned at 50 mm, also at time, t. The N_C curve at 50 mm will thus be a horizontal line with a value of 1.0. The 50 mm depth was chosen to benchmark all conductivity values since it primarily reflects hydration effects, and is not influenced to any great extent by surface wetting and drying (or NaCl ingress), at this stage.

Figs. 10 and 11 present this parameter over the test period for, respectively, water- and NaCl-exposed samples. Wetting and drying cycles are still clearly evident; however, the most striking effect is the influence of NaCl on N_C in comparison to the respective water-exposed specimens, particularly over the surface 0–10 mm. This feature is not so pronounced on the respective conductivity versus time response presented in Figs. 2 and 3.

Several processes will influence conductivity, hence N_C: hydration, pozzolanic reaction, chloride binding and drying effects all serving to decrease N_C, with water ingress increasing N_C, enhanced by the presence of NaCl in the pore fluid. In the long term i.e. once hydration and pozzolanic activity has ceased, conductivity will be a function of both level of pore saturation and pore-fluid

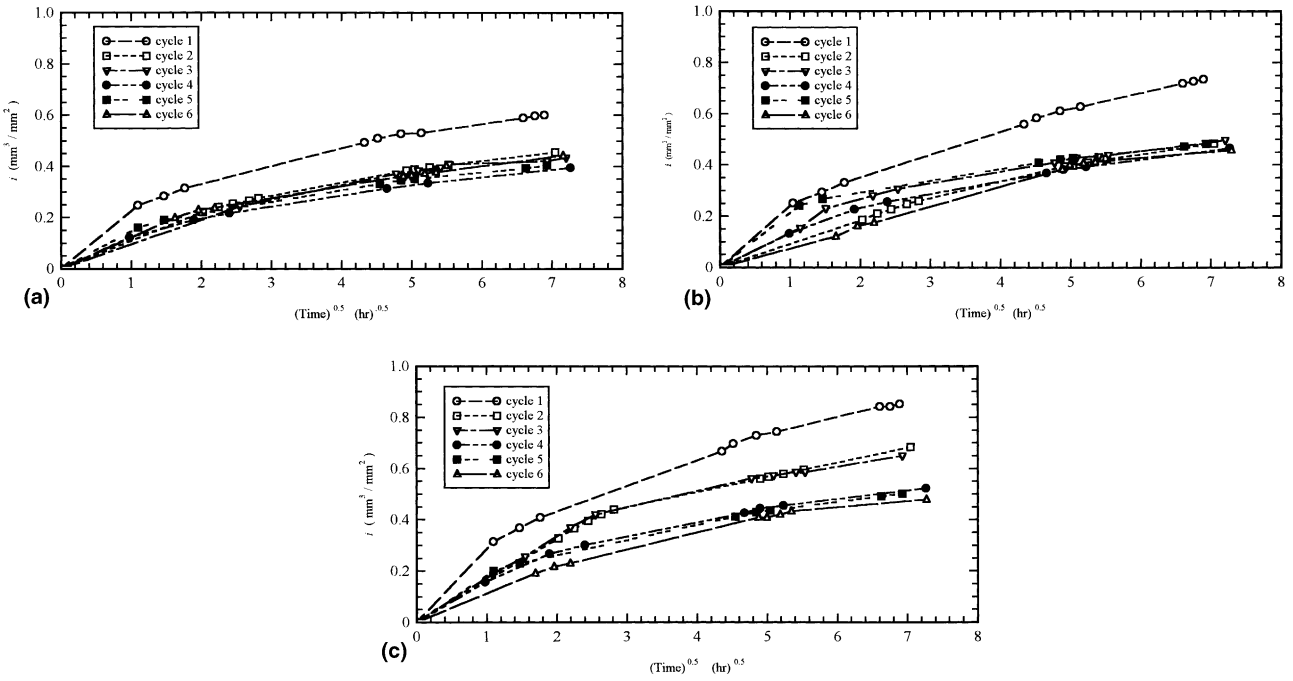

Fig. 8. Cumulative volumetric gain of specimens over initial six wetting cycles for (a) OPC, (b) GGBS, and (c) PFA (water).

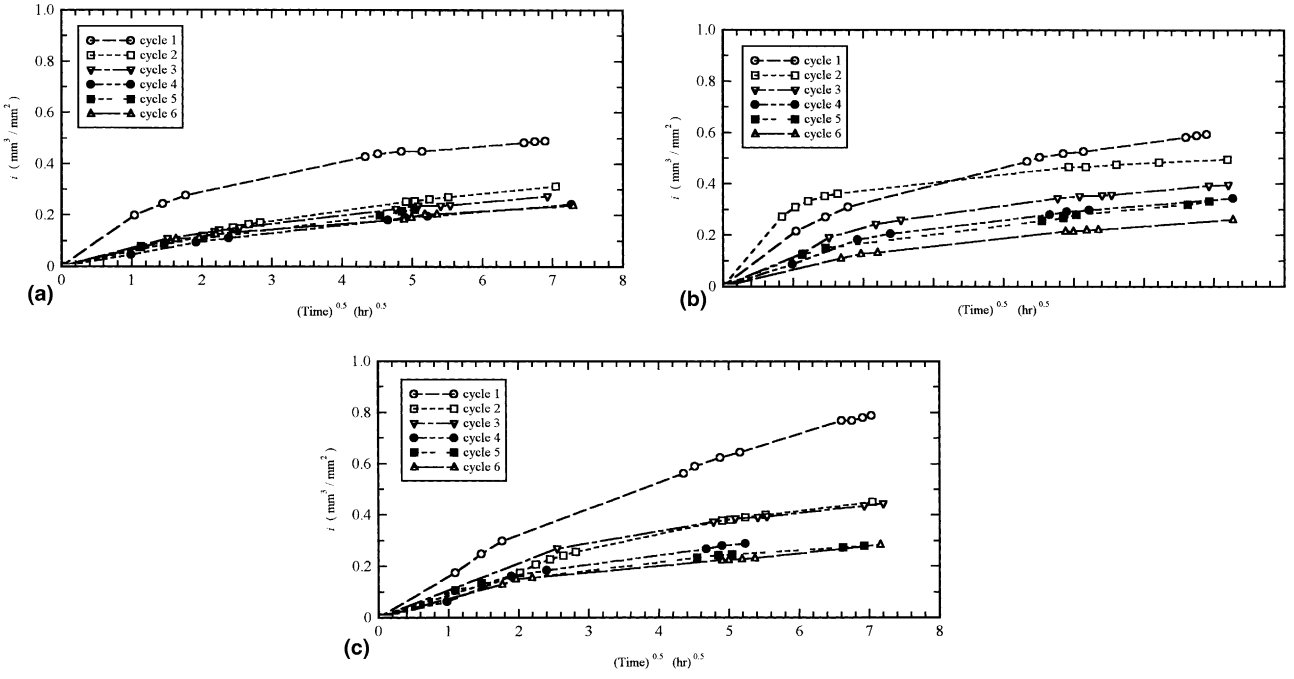

Fig. 9. Cumulative volumetric gain of specimens over initial six wetting cycles for (a) OPC, (b) GGBS, and (c) PFA (NaCl).

conductivity. If the level of saturation fluctuates due to cycles of wetting and drying, the conductivity will change in sympathy; if monitored over time, the conductivity will tend to fluctuate about a zone defined by the maximum/minimum values after wetting/drying respectively, this zone remaining relatively constant. This is evident in Fig. 10 for the water-exposed samples. The water-exposed PFA (Fig. 10(c)) displays N_C values at 5 mm which consistently peak above the benchmark value of 1.0 (at 50 mm) and we associate this feature with a more porous surface zone due to the susceptibility of this replacement material to curing conditions.

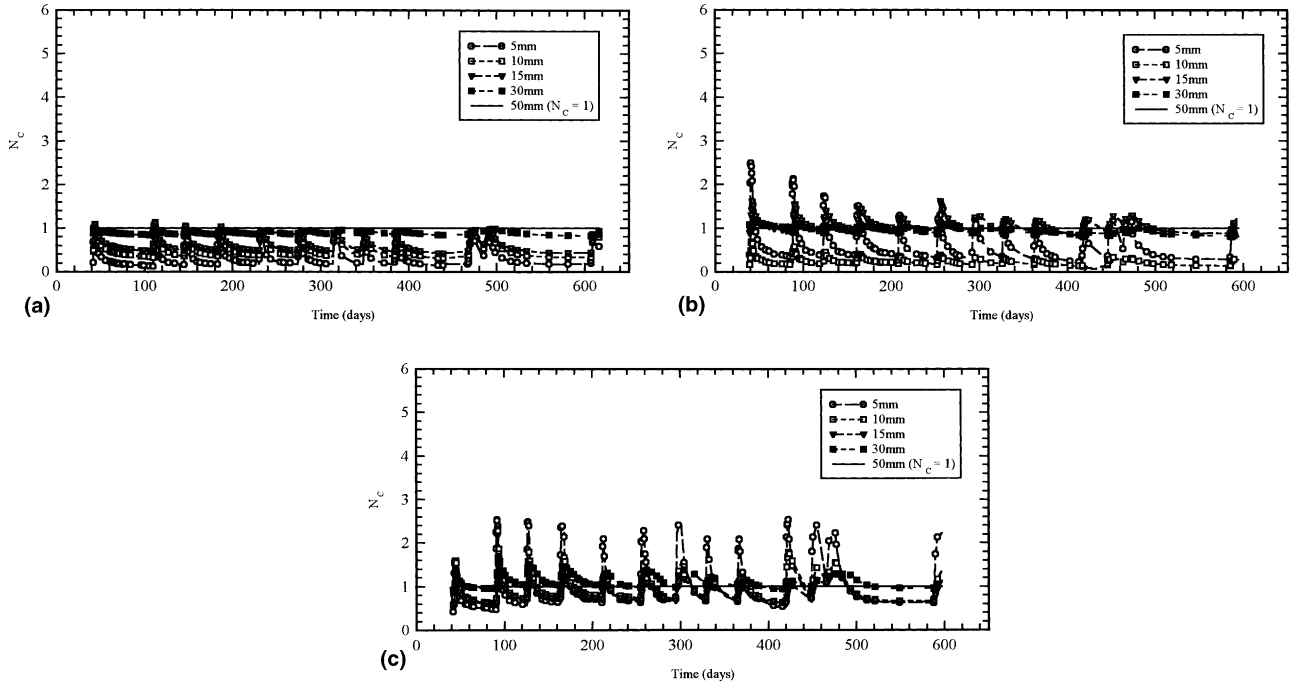

Fig. 10. Variation of N_C over cycles of wetting and drying for (a) OPC, (b) GGBS, (c) PFA (water).

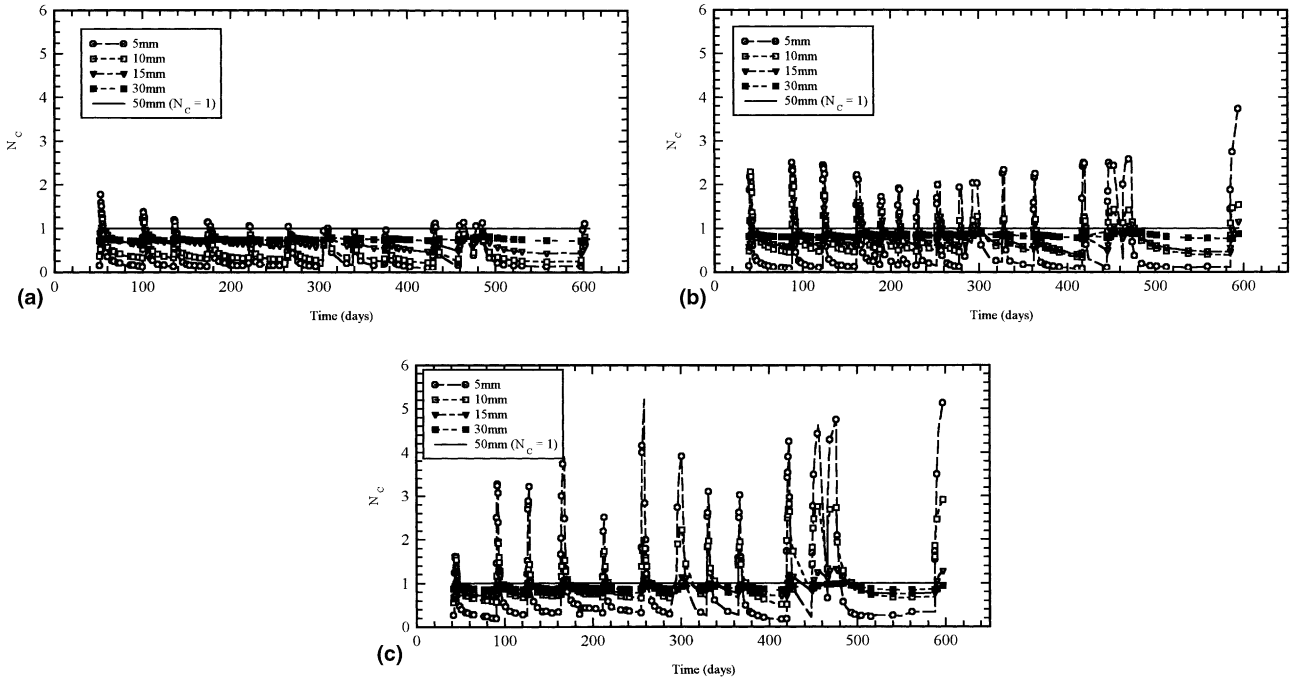

Fig. 11. Variation of N_C over cycles of wetting and drying for (a) OPC, (b) GGBS, (c) PFA (NaCl).

If the invading water contains dissolved ionic species, then cycles of wetting and drying will cause the conductivity to fluctuate between a zone which gradually increases with time as each electrode pair responds to the increasing NaCl concentration in the pore water. This is evident in Fig. 11 towards the end of the period presented. N_C values indicate ionic ingress into the surface 0–5 mm for the OPC mix (Fig. 11(a)); on the other hand, GGBS and PFA show NaCl enrichment of the surface 0–10 mm. As the NaCl advances into the

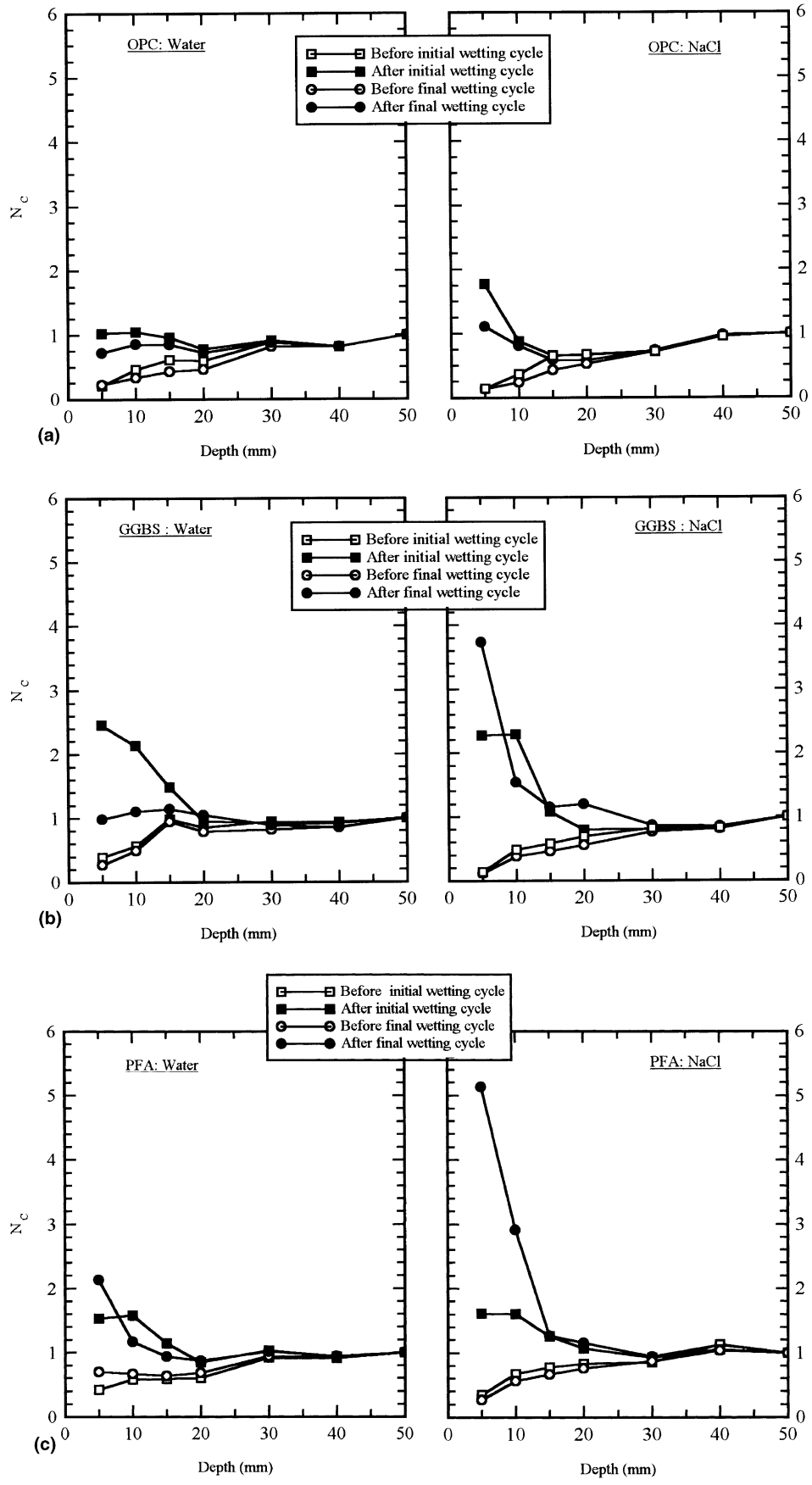

Fig. 12. Initial and final N_C versus depth profiles (before/after wetting) for (a) OPC specimens; (b) GGBS specimens; and (c) PFA specimens.

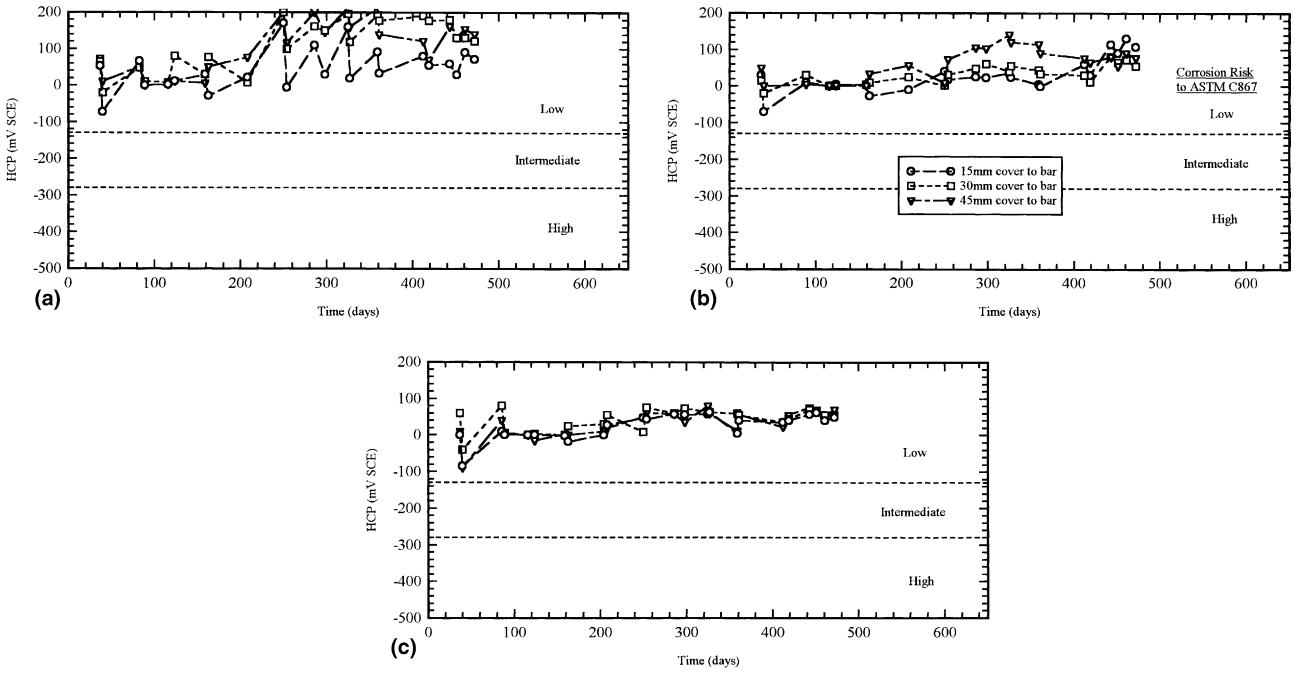

Fig. 13. Half-cell potential for steel bars at 15, 30 and 45 mm from surface for (a) OPC, (b) GGBS, and (c) PFA (water).

covercrete the conductivity, hence N_C, at each pair of electrodes will increase in response to the increasing ionic concentration within the pore fluid. This allows tracking of the chloride front. This feature is further highlighted in Figs. 12(a)–(c), where N_C is plotted as a function of depth through the surface 50 mm. Profiles are presented both before and after the initial and final wetting cycles. Increasing ionic concentration within the surface 0–5 mm for OPC and 0–10 mm for both GGBS and PFA is apparent.

3.5. Half-cell measurements

In parallel with conductivity measurements, half-cell potentials of the embedded steel bars (vs. SCE) are

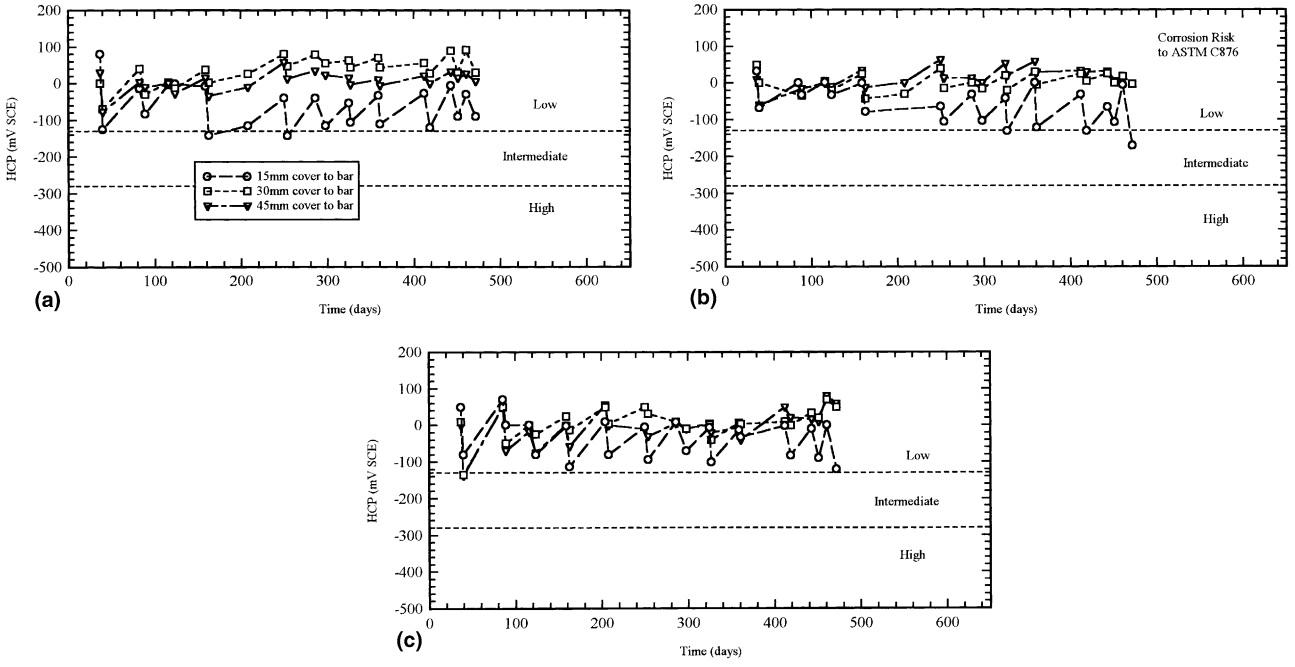

Fig. 14. Half-cell potential for steel bars at 15, 30 and 45 mm from surface for (a) OPC, (b) GGBS, and (c) PFA (NaCl).

presented in Figs. 13 and 14 for water and NaCl exposure, respectively. For water exposure, all bars indicate no risk of corrosion, as would be expected. Specimens exposed to NaCl solution show no risk of corrosion for bars with a 30 and 45 mm cover, and a low risk for the bar with 15 mm cover in the case of the OPC concrete. The GGBS and PFA concretes indicate a transition from low- to intermediate risk of corrosion for the bar with 15 mm cover. This would support N_C measurements as they indicated NaCl enrichment in the surface 0–5mm for OPC, and the surface 0–10 mm for GGBS and PFA. N_C values indicate that ionic ingress had not yet penetrated to the depth of the next respective electrode-pair position in sufficient quantities to increase the conductivity to any measurable extent (i.e. 10 mm for OPC, and 15 mm for GGBS and PFA). However, with continued wetting cycles this situation would be expected to change for reasons discussed above.

4. Concluding comments

An experimental programme was undertaken on concrete mixes designed for extreme exposure conditions. The work detailed has shown that discretized electrical measurements (conductivity in this instance) within the cover concrete can be used to study the spatial distribution of salient features that have an important influence on concrete durability. In addition, a normalised conductivity parameter was introduced to study the effect of water and ionic ingress. The conductivity at a depth of 50 mm was used to benchmark all subsequent conductivity values. Unlike electrodes positioned within the surface 30 mm, the wetting and drying regime applied to the concrete surface did not cause a marked response at the electrodes positioned at 50 mm. It was shown that, over the test period, the response at 50 mm remains relatively unaffected by wetting and drying action at the surface and reflects hydration effects.

By studying conductivity profiles just prior to absorption and immediately after absorption allowed evaluation of that zone of cover most influenced by wetting and drying action. It was shown that for the drying and wetting regime employed, the convective zone extended to approximately 30 mm, although this reduced with time. In the longer term, as the influence of hydration on conductivity diminishes, the level of saturation of the connected pore system and the pore fluid conductivity (hence concentration of invading ions) will dominate the measured conductivity. This is particularly evident for the PFA samples subjected to NaCl where, at the end of the test period, there is an enhancement in the conductivity over the surface 10 mm.

Acknowledgements

The authors wish to acknowledge the financial support of the Engineering and Physical Sciences Research Council (EPSRC) (Grant GR/L55810).

References

[1] Figg JW. Methods for measuring the air and water permeability of concrete. Mag Concr Res 1973;25(85):213–9.
[2] British Standards Institution (London, UK), BS 1881: Part 122 Method for determination of water absorption, 1983, 4p.
[3] Dhir RK, Hewlett PC, Chan YN. Near-surface characteristics of concrete: assessment and development of in situ test methods. Mag Concr Res 1987;39(141):183–95.
[4] Hall C, Yau MHR. Water movement in porous building materials – IX: the water absorption and sorptivity of concretes. Build Environ 1987;22:77–82.
[5] Meletion CA, Tia M, Bloomquist D. Development of a field permeability test apparatus and method for concrete. ACI Mater J 1992;89(1):83–9.
[6] British Standards Institution (London, UK), BS 1881: Part 208 Recommendations for the determination of the initial surface absorption of concrete, 1996, 14p.
[7] Wilson MA, Taylor SC, Hoff WD. The initial surface absorption test (ISAT): an analytical approach. Mag Concr Res 1998; 50(2):179–85.
[8] Basheer PAM. A brief review of methods for measuring the permeation properties of concrete in situ. Proc Inst Civ Eng (London, UK): Build Struct 1993;99:74–83.
[9] Blight GE, Lampacher BJ. Applying covercrete absorption test to in-situ tests on structures. ASCE J Mater Civ Eng 1995;7(1):1–8.
[10] Classie PA, Elsayad HI, Shaaban IG. Test methods for measuring fluid transport in cover concrete. ASCE J Mater Civ Eng 1999;11(2):138–43.
[11] European Union – Brite EuRam III, Duracrete – Modelling of degradation. Report BE95-1347/R4-5, 1998, December, 174pp [ISBN 90 376 0444 7].
[12] European Union – Brite EuRam III, Duracrete – Models for environmental actions on concrete structures. Report BE95-1347/R3, 1999, March, 273pp [ISBN 90 376 0400 5].
[13] Bracs G, Balint E, Orchard DF. Use of electrical resistance probes in tracing moisture permeation through concrete. J Amer Concr Inst 1970;67(8):642–6.
[14] Sriravindrarajah R, Swamy RN. Development of a conductivity probe to monitor setting time and moisture movement in concrete. ASTM, Cem, Concr Aggregates 1982;4(2):73–80.
[15] Schießl P, Raupach M. New approaches for monitoring the corrosion risk for the reinforcement – installation of sensors. In: Proceedings of the Concrete across Borders Conference, vol. 1, 1994; Odense, Denmark. p. 65–77.
[16] McCarter WJ, Emerson M, Ezirim H. Properties of concrete in the cover zone: developments in monitoring techniques. Mag Concr Res 1995;47(172):243–51.
[17] McCarter WJ, Brousseau R. The AC response of hardened cement paste. Cem Concr Res 1990;20(6):891–900.
[18] Tuutti K. Effect of cement type and different additions on service life. In: Dhir RK, Jones MR, editors. Proceedings of the Concrete 2000 Conference, vol. 2. London, UK: E&FN Spon; 1993. p. 1285–95.
[19] Alonso C, Andrade C, Gonzalez JA. Relation between resistivity and corrosion rate of reinforcements in carbonated mortar made with several cement types. Cem Concr Res 1988;8(5):687–98.

[20] Sagoe-Crentsil KK, Glasser FP. Steel in concrete: Part I A review of the electrochemical and thermodynamic aspects. Mag Concr Res 1989;41(149):205–12.
[21] Millard SG, Gowers KR. Resistivity assessment of in-situ concrete: the influence of conductive and resistive surface layers. Proc Inst Civ Eng: Struct Build 1992;94:389–96.
[22] Lopez W, Gonzalez JA. Influence of degree of saturation on the resistivity of concrete and the corrosion rate of steel reinforcement. Cem Concr Res 1993;23(2):368–76.
[23] Broomfield JP. Corrosion of steel in concrete. London: E&FN Spon; 1997. 240pp [ISBN 0 419 19630 7].
[24] McCarter WJ, Ezirim H, Emerson M. Absorption of water and chloride into concrete. Mag Concr Res 1992;44(158):31–7.
[25] Midgley HG, Illston JM. The penetration of chlorides into concrete. Cem Concr Res 1984;14(4):546–58.
[26] Suryavanshi AK, Scantlebury JD. Pore size distribution of OPC and SRPC mortars in presence of chlorides. Cem Concr Res 1995;25(5):980–8.